NONLOCAL FRACTIONAL DYNAMICS FOR DIFFERENT TERMINAL DENSITIES

J.L. Silva

Centro de Investigação em Matemática e Aplicações, University of Madeira
9020-105 Funchal, Madeira, Portugal

V.A. Stephanovich

Institute of Physics, Opole University, Oleska 48, 45-052 Opole, Poland

(Received March 9, 2018; accepted April 10, 2018)

We study the effect of confining potentials, generated by different equilibrium (long-time asymptotic or terminal) probability densities, on non-Gaussian stochastic processes, described by Lévy–Schrödinger semigroup dynamics. The former densities belong to the family of so-called $\mathbb{M}$-Wright functions of index ν. Using analytical and numerical arguments, we demonstrate that properly tailored confining potentials can generate the Gaussian distribution (which is also a member of $\mathbb{M}$-Wright family at $\nu = 1/2$) at final stages of time evolution. This means that the Gaussian distribution (and other sufficiently fast decaying distributions like exponential one) can emerge in the differential equation with fractional derivatives, which normally produces the heavy-tailed, slow-decaying probability densities. We discuss the physical implications of the results obtained, for instance, in the evolution of magnetic resonanse lineshapes for complex, multi-peaked resonant lines.

DOI:10.5506/APhysPolB.49.1607

1. Introduction

The differential equations containing fractional derivatives are very convenient to describe the dynamics of probabilistic systems. The main point here is that standard techniques for solving partial differential or integral equations also apply to fractional equations. These equations are usually solved for probability density functions (pdf) or quantities directly related to them. The ubiquity of Gaussian and non-Gaussian random walks in the Nature makes them a subject of intensive studies in mathematics [1–3], physics [3, 4], chemistry [4], economy [5, 6], biology and earth sciences [7–9].

In general, the temporal evolution of the above complex systems deviates from the corresponding standard laws described, for example, by ordinary Fokker–Planck equations, see, *e.g.* [10] for recent review. The advancement of experimental techniques (like resonant spectroscopies, see below) makes these deviations more accessible and by this virtue, it becomes possible to deduce the physical laws governing the random motions.

Dealing with the diffusion processes, involving fractional derivatives, one usually arrives at the so-called generalized diffusion equation

$$\partial_t \theta(x,t) = -\mathcal{H}\theta(x,t)\,, \tag{1}$$

where $\theta(x,t)$ is interpreted as a wave function (related to the pdf of a system, see below) and $\mathcal{H}$ is a Hamiltonian operator, which will be defined explicitly below. The latter means that, apart from the absence of imaginary unit in time derivative, the generalized diffusion equation can be regarded as Schrödinder-type one. In its turn, the Hamiltonian operator is a generator $\exp(-t\mathcal{H})$ of the dynamical Lévy–Schrödinder semigroup, see Ref. [1] for detailed mathematical explanation of this concept. We note that asymmetric (*i.e.* one-sided or defined either on positive or negative real semiaxis) stable processes cannot be transformed into a semigroup dynamics [11]. That is why here, we will use the symmetrized semigroup potentials, defined as even functions in the whole real axis.

The common knowledge about fractional derivatives is that they generate the heavy-tailed, non-Gaussian pdfs, especially in the dynamical patterns. Namely, even if the initial (at $t = 0$) pdf is Gaussian, the final stages of its time evolution yield the pdfs with only finite number of moments in existence (see, *e.g.* [12, 13]). Contrary to that here, we show that the proper choice of external potential in the above generalized diffusion equation generates Gaussian pdf as the large time asymptotics of the fractional diffusion.

For that we employ a so-called one parametric (with parameter $0 \leq \nu \leq 1$) $\mathbb{M}$-Wright family of the pdfs [14, 15]. At $1 \leq \nu < 0.5$, the symmetrized $\mathbb{M}(|x|)$-Wright family functions have two-peak shape, resembling the letter M, hence the name. This family, in turn, is the special case of two-parametric Wright function, which had been introduced by British mathematician E.M. Wright [16–18] in the asymptotic theory of partitions. The function we are interested in can be defined by following power series [15]:

$$\mathbb{M}_\nu(z) = \sum_{n=0}^{\infty} \frac{(-1)^n z^n}{n!\Gamma[1-\nu(n+1)]}\,, \tag{2}$$

where $\Gamma(s)$ is gamma-function [19] and z is, generally speaking, a complex variable. In subsequent discussion, we will be interested in the symmetrized,

even version $\mathbb{M}_\nu(|x|)$ of functions (2), where $x \in \mathbb{R}$ is real. For special values of ν, functions (2) can be expressed through the known functions

$$\mathbb{M}_0(|x|) = e^{-|x|}, \qquad \mathbb{M}_{1/2}(|x|) = \frac{1}{\sqrt{\pi}} \exp\left[-\frac{x^2}{4}\right],$$
$$\mathbb{M}_1(|x|) = \frac{1}{2}\left[\delta(x-1) + \delta(x+1)\right]. \tag{3}$$

We plot the family $\mathbb{M}_\nu(|x|)$ in Fig. 1. The characteristic M-like shape at $\nu > 0.5$ is clearly seen. We can also see the evolution from exponential function with cusp (due to symmetrization) at $\nu = 0$ through Gaussian at $\nu = 0.5$ to two-peaked δ function, shown in the inset. Below, applying the Lévy targeting method elaborated earlier [20], we use function (3) to construct semigroup potential and hence the dynamic relaxation patterns.

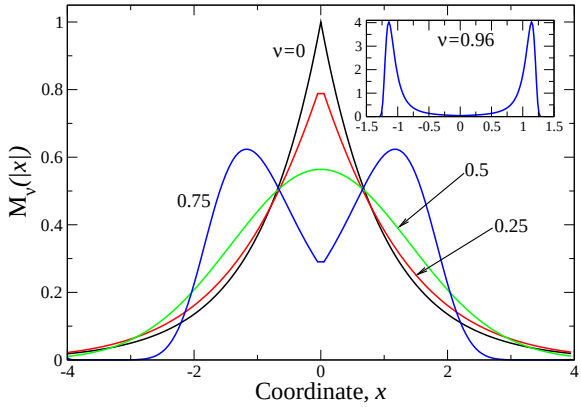

Fig. 1. $\mathbb{M}$-Wright family of functions $\mathbb{M}_\nu(|x|)$ for different values of ν, shown in the main panel as figures near curves. The inset reports the function $\mathbb{M}_{0.96}(|x|)$, which is close to two-peaked δ function. The vertical scale is much larger then that for smaller ν.

The renewed interest to the $\mathbb{M}$-Wright family of the functions [14, 15] is related to the fact that, along with Mittag–Leffler function [15] (see also Ref. [21], where the interrelation between two functions is discussed), it is the solution of the equation

$$\frac{\partial^\alpha u(x,t)}{\partial t^\alpha} = D_\alpha \frac{\partial^2 u(x,t)}{\partial x^2}, \qquad D_\alpha > 0, \qquad 0 < \alpha \le 2, \tag{4}$$

which represents the ordinary free (*i.e.* without external potentials) diffusion equation, where the first time derivative is substitituted by fractional (of the order of α) Caputo (or Riemann–Liouville) [14] one

$$\frac{\partial^{\alpha}u(x,t)}{\partial t^{\alpha}}=\begin{cases}\frac{\partial^{n}u(x,t)}{\partial t^{n}}, & \alpha=n\in N\,,\\ \frac{1}{\Gamma(n-\alpha)}\int\limits_{0}^{t}(t-t')^{n-1-\alpha}\,\frac{\partial^{n}u(x,t)}{\partial t^{n}}\mathrm{d}t', & n-1<\alpha<n\,.\end{cases}\tag{5}$$

In Eq. (4), D_α is also a sort of diffusion coefficient with dimensions $\mathrm{cm}^2/\mathrm{sec}^\alpha$.

In this case, the solution of equation (4) can be represented either in terms of Mittag–Leffler or $\mathbb{M}$-Wright functions, see Refs. [14, 15, 21] for details. As in equation (4) the spatial derivative (ordinary Laplacian) is left intact, this equation can be regarded as Brownian motion like process with distinctive (due to substitution of the ordinary time derivative by fractional one) dynamics. The main feature of such dynamics is nonlinear (sub- or superlinear) time growth of a spatial variance of corresponding pdf. The term "time-fractional diffusion" in this case is attributed to, say, super- and subdiffusions, see Ref. [1]. In pinciple, one may use the Lévy targeting strategy of Ref. [20] to the studies of dynamics, governed by equation (4) in the (properly chosen, see below) external potentials. Interesting question is also an interplay between fractional time and spatial derivatives in the above dynamics in the external potentials. We postpone the discussion of these questions to the future publications.

In the present paper, we show that albeit functions (2) appear as the solution of equation (4) with time-fractional derivative (5), they can be well-used in the above Lévy–Schrödinder semigroup framework, which describes discontinuous, jump-type processes [1]. This permits to represent the targets of the corresponding motion in terms of $\mathbb{M}_\nu(x)$ functions family. Below, we show that as a result of the semigroup dynamics, the initial two-peak distribution, almost equal to $\mathbb{M}_1(x)$, relaxes either to Gaussian pdf $\mathbb{M}_{1/2}(|x|)$ or to exponential one $\mathbb{M}_0(|x|)$. This is the case for the dynamics of inhomogeneously broadened magnetic resonance spectral lines (see, *e.g.* [22]), which we are going to study in detail in future publications. The other physically important examples where $\mathbb{M}$-Wright family can be used are listed in the final part of the paper.

2. General formalism

To make the dynamics set by Eq. (1) explicit, we define the Hamiltonian operator in the Lévy–Schrödinger form

$$\mathcal{H}\equiv\mathcal{H}_\mu=\lambda|\Delta|^{\mu/2}+\mathcal{V}(x)\,,\tag{6}$$

where $\lambda>0$ is the so-called intensity parameter of the Lévy process (see, *e.g.* Ref. [12]). Here, we consider the nonlocal fractional generalization of the ordinary Laplacian $-|\Delta|^{\mu/2}$, $0<\mu<2$, defined as (see, *e.g.* [23])

$$-|\Delta|^{\mu/2} f(x) = A_\mu \int\limits_{\mathbb{R}} \frac{f(y) - f(x)}{|x-y|^{\mu+1}}\, \mathrm{d}y\,, \tag{7}$$

where the normalizing constant A_μ is given by

$$A_\mu = \frac{\Gamma(1+\mu)\sin\frac{\pi\mu}{2}}{\pi}\,. \tag{8}$$

Note that integral in (7) is understood in the sense of its Cauchy principal value, see Ref. [20] for details. For $-\mathcal{H}_\mu$ to be a legitimate generator of a dynamical semigroup [24], the external potential $\mathcal{V}(x)$ should be bounded from below [24].

Looking for stationary solutions of the semigroup equation (1) with Hamiltonian (6), we see that if a square root of a terminal (final, invariant) pdf $\rho_*(x)$ realizes the long-time ($t \to \infty$) asymptotics of semigroup dynamics, then the resulting fractional static Sturm–Liouville equation

$$\mathcal{H}_\mu \rho_*^{1/2} \equiv \lambda |\Delta|^{\mu/2} \rho_*^{1/2} + \mathcal{V}\rho_*^{1/2} = 0 \tag{9}$$

generates following compatibility condition in the form of $\mathcal{V}(x)$ [12, 20]

$$\mathcal{V}(x) \equiv \mathcal{V}_\mu(x) = -\lambda \frac{|\Delta|^{\mu/2}\rho_*^{1/2}(x)}{\rho_*^{1/2}(x)}\,. \tag{10}$$

The semigroup dynamics with potential (10) gives a solution for the so-called *targeting problem*, with the target being the predefined terminal pdf. On the other hand, defining a specific potential $\mathcal{V}(x)$, we infer the invariant pdf $\rho_*^{1/2}(x)$ from the static equation (9). This problem is called *reverse engineering problem* [25]. Here, we will consider the targeting problem for terminal pdfs belonging to above $\mathbb{M}$-Wright family of functions.

To derive the explicit expressions for $\mathcal{V}_\mu(x)$ for different terminal pdfs $\rho_*(x)$, we use the Fourier technique, which is appropriate for the case of unbounded motion. The detailed derivation of the corresponding formulas can be found, for instance, in Ref. [26]. Their result is that the Fourier image of our fractional derivative (7) is $|k|^\mu$.

We first derive the potential $\mathcal{V}_\mu(x)$ for the Gaussian terminal pdf, related to $\mathbb{M}_{1/2}(|x|)$. Its explicit form reads

$$\rho_*(x) = \frac{1}{2}\mathbb{M}_{1/2}(|x|) = \frac{1}{2\sqrt{\pi}} e^{-\frac{x^2}{4}}\,. \tag{11}$$

Note that coefficient $1/2$ before $\mathbb{M}_{1/2}(|x|)$ has been chosen for $\rho_*(x)$ to be normalized to unity, *i.e.*

$$\int\limits_{-\infty}^{\infty} \rho_*(x)\mathrm{d}x = 1\,. \tag{12}$$

The Fourier image of square root $\rho_*^{1/2} = (2\sqrt{\pi}\,)^{-1/2} e^{-x^2/8}$ reads

$$f(k) = \left(\frac{4}{\pi}\right)^{1/4} e^{-2k^2}. \tag{13}$$

Substitution of Eq. (13) into the integral for inverse Fourier image generates the following form of semigroup potential:

$$\mathcal{V}_{\mu\mathrm{G}}(x) = -\lambda\sqrt{\frac{2}{\pi}}\, e^{x^2/8} \int\limits_{-\infty}^{\infty} |k|^{\mu} e^{-2k^2} e^{-ikx}\mathrm{d}x\,, \tag{14}$$

which finally yields (see also Ref. [20]), where the case of Gaussian with arbitrary variance σ has been considered

$$\mathcal{V}_{\mu\mathrm{G}}(x) = -\frac{2^{-\frac{\mu}{2}}}{\sqrt{\pi}}\Gamma\left(\frac{\mu+1}{2}\right) {}_1F_1\left(-\frac{\mu}{2}; \frac{1}{2}; \frac{x^2}{8}\right), \tag{15}$$

where ${}_1F_1(\dots)$ is a confluent hypergeometric function, see Ref. [19]. Note that expression (15) can be obtained also explicitly, *i.e.* without Fourier technique, from the integral

$$\int\limits_{-\infty}^{\infty} \frac{e^{-\frac{y^2}{8}} - e^{-\frac{x^2}{8}}}{|x-y|^{1+\mu}}\mathrm{d}y = \int\limits_{-\infty}^{\infty} \frac{e^{-\frac{(x-y)^2}{8}} - e^{-\frac{x^x}{8}}}{|y|^{1+\mu}}\mathrm{d}y$$
$$= 2^{-\frac{3\mu}{2}}\Gamma\left(-\frac{\mu}{2}\right) {}_1F_1\left(\frac{\mu+1}{2}; \frac{1}{2}; -\frac{x^2}{8}\right),$$

which is more laborius in computation as we should observe the Cauchy principal value for it.

In Fig. 2, we report the plots of $\mathcal{V}_{\mu\mathrm{G}}(x)$ (15) for $\mu \in \{0, 0.5, 1.0, 1.5, 2.0\}$. It is seen that at $\mu = 0$, $\mathcal{V}_{\mu\mathrm{G}}(x) = -1$ as it follows from definition (10). Really, at $\mu = 0$, the derivative of zeroth order gives the function $\rho_*^{1/2}(x)$ itself, which cancels out with the denominator of fraction in Eq. (10). As $\mu < 1$ grows, the potential has the shape with flat bottom and steep walls. It is always limited from below, as should be for "correct" semigroup potential. At $\mu > 1$, the growth becomes slower and finally at $\mu = 2$, it arrives at parabolic asymptotics

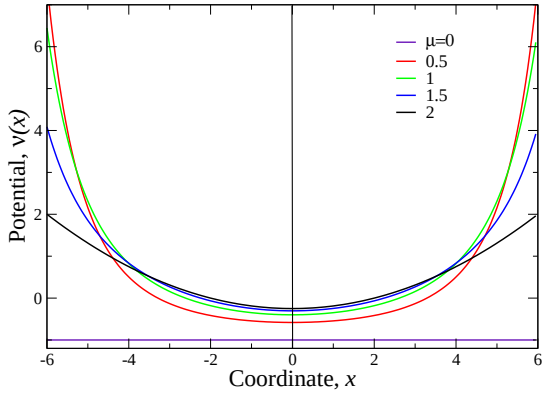

Fig. 2. (Colour on-line) Potential $\mathcal{V}_{\mu\mathrm{G}}(x)$ for Gaussian terminal pdf (11). Here, $\lambda = 1$ and values of Lévy index μ are shown in the legend.

$$\mathcal{V}_{\mu=2,\mathrm{G}} = -\frac{1}{4}\left(1 - \frac{x^2}{4}\right).$$

The latter asymptotics can be easily obtained either from definition (10), where we have second derivative in this case, or from (15), where hypergeometric function ${}_1F_1(-1, 1/2, x^2/8)$ reduces to second Hermitian polynomial H_2 [19].

Next, we derive the expression for the semigroup potential $\mathcal{V}_{\mu\mathrm{E}}$ for the exponential pdf

$$\rho_*(x) = \frac{1}{2}e^{-|x|}, \tag{16}$$

stemming from the symmetrized density, generated by the function $\mathbb{M}_0(|x|) = e^{-|x|}$. Once more, the normalization to unity (12) is respected. The Fourier image $f(k)$ for $\rho_*^{1/2} = e^{-|x|/2}/\sqrt{2}$ reads

$$f(k) = \frac{1}{2\sqrt{\pi}} \int\limits_{-\infty}^{\infty} e^{-|x|/2} e^{\imath kx} \mathrm{d}x = \frac{2}{\sqrt{\pi}} \frac{1}{1+4k^2}. \tag{17}$$

In this case, $\mathcal{V}_{\mu\mathrm{E}}(x)$ assumes the following integral form:

$$\mathcal{V}_{\mu\mathrm{E}}(x) = -\frac{2\lambda}{\pi} e^{|x|/2} \int\limits_{-\infty}^{\infty} \frac{|k|^\mu \cos kx}{1+4k^2} \mathrm{d}k = \frac{\lambda}{\pi} e^{|x|/2} \left[\frac{\pi}{2^\mu \cos\frac{\pi\mu}{2}} \cosh\frac{x}{2} + \frac{\Gamma(\mu-1)\sin\frac{\pi\mu}{2}}{x^{\mu-1}} \, {}_1F_2\left(1, \left\{1 - \frac{\mu}{2}, \frac{3-\mu}{2}\right\}, \frac{x^2}{16}\right)\right]. \tag{18}$$

Integral (18) has been calculated in Mathematica; ${}_1F_2(\dots)$ is a generalized hypergeometric function [19].

The plots of potential (18) for $\lambda = 1$ and different μ are shown in Fig. 3. We pay attention here that since function (18) has removable divergencies at $\mu = 0, 1$ and 2, we calculate the corresponding dependences for $\mu = 0.001$, 0.9999 and 1.9999, respectively. It is seen that for $\mu = 0$, similar to the case of Gaussian function, the potential $\mathcal{V}_0(x) = -1$, while for $\mu = 2$, we have correct asymptotics $\mathcal{V}_2(x) = 1/4$. Panel (a) shows that at each μ, except exactly 0 and 2, the potential has cusp-like peculiarity near $x = 0$. This peculiarity is due to modulus sign ("nib-like" shape near $x = 0$) in the terminal pdf (16), see also Fig. 1. We note here that contrary to the case of Gaussian terminal pdf (11), the asymptotics at $\mu = 2$ is constant similar to the common case $\mu = 0$.

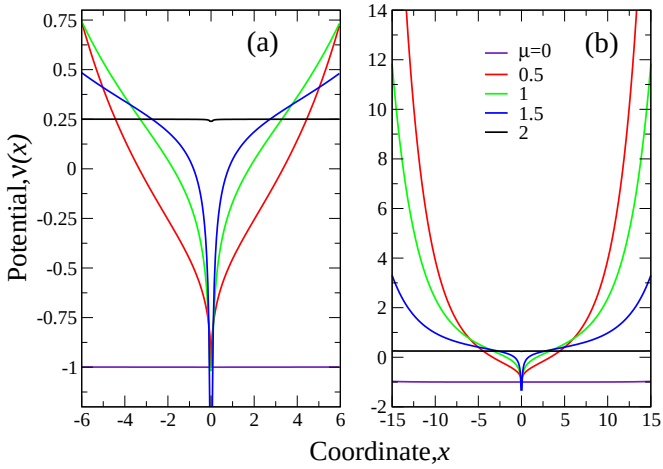

Fig. 3. Potential $\mathcal{V}_{\mu\mathrm{E}}(x)$ for exponential terminal pdf (16) at $\lambda = 1$ and different values of μ, shown in panel (b). Panel (a) reports the details at relatively small x, while panel (b) shows the general shape of the potential.

3. Large $|x|$ asymptotics of the semigroup potentials

To verify the consistency of our Lévy targeting approach, it is instructive to check analytically the spatial asymptotic behaviour of the target pdfs $\rho^*(x)$, given by expressions (11) and (16). Both pdfs, similar to other members of $\mathbb{M}_\nu(x)$ family, can be considered as ground states of operator (6). Using this property, the authors of Ref. [27] (see also [28]) arrived at the following general asymptotic relation:

$$(\rho^*)^{1/2}(x \to \infty) \sim \frac{1}{\mathcal{V}_\mu(x)|x|^{1+\mu}}\,, \tag{19}$$

where $\mathcal{V}_\mu(x)$ is the above semigroup potential.

To derive the asymptotic relations for our terminal pdfs $\rho^*(x)$, we can use the methodology of Sec. III of Ref. [27]. It uses the fact that the functions $\sqrt{\rho^*(x)}$ form ground state of operator (6), which should exist as the potential $\mathcal{V}_\mu(x)$ is unbounded from above. However, the more profitable way is to derive relation (19) explicitly via the asymptotics of semigroup potentials, corresponding to each of our final pdfs (11) and (16).

We begin with Gaussian pdf (11). For that, we use following asymptotic relation for confluent hypergeometric function [19]:

$$ {}_1F_1(a, b, z \to \infty) \approx \frac{\Gamma(b)}{\Gamma(a)} z^{a-b} e^z \,. $$

Applying this expression to potential (15), we obtain

$$ {}_1F_1\left(-\frac{\mu}{2}; \frac{1}{2}; \frac{x^2}{8}\right)\Bigg|_{x\to\infty} \approx \frac{\sqrt{\pi}\; e^{x^2/8}\; 2^{3(1+\mu)/2}}{\Gamma(-\mu/2)|x|^{1+\mu}} \,. \tag{20} $$

On the other hand, from Eq. (11), we have

$$ e^{x^2/8} = \frac{1}{\pi^{1/4}\sqrt{2}\sqrt{\rho^*}} \,. \tag{21} $$

Substitution of asymptotic expression (20) with respect to Eq. (21) into (15) yields (lower index G stands for "Gaussian")

$$ \mathcal{V}_{\mu\mathrm{G}}(x \to \infty) \approx -\frac{\pi^{1/4}}{\Gamma(-\mu)\cos\frac{\pi\mu}{2}|x|^{1+\mu}\sqrt{\rho^*(x)}} \,. \tag{22} $$

Expression (22) renders immediately to the desired form of asymptotics for the Gaussian target pdf

$$ (\rho^*)^{1/2}_{\mathrm{G}}(x \to \infty) \approx -\frac{\pi^{1/4}}{\Gamma(-\mu)\cos\frac{\pi\mu}{2}\;|x|^{1+\mu}\mathcal{V}_{\mu\mathrm{G}}(x)} \,. \tag{23} $$

We notice that as $\Gamma(-\mu)\cos\frac{\pi\mu}{2} < 0$ for $2 < \mu < 0$, quantity (23) is positive as it should be. We see that our method gives not only the leading term of asymptotic expansion (19), but also the coefficient before it. To derive expression (22), we use the following relation for Γ functions [19]:

$$ \frac{\Gamma((1+\mu)/2)}{\Gamma(-\mu/2)} = \frac{\sqrt{\pi}\; 2^{-(1+\mu)}}{\Gamma(-\mu)\;\cos\frac{\pi\mu}{2}} \,. $$

Now, we consider the asymptotics of exponential pdf (16). It turns out that, similar to the calculation of the semigroup potential (18), this case is

more mathematically intricate then that for Gaussian target. For instance, there is no simple asymptotic formula for hypergeometric function ${}_1F_2(\dots)$. To calculate the large x asymptotics in this case, we make the substitution $kx = t$ in integral (18), which yields (lower index E stands for "exponential")

$$\mathcal{V}_{\mu\mathrm{E}}(x) = -\frac{2\lambda}{\pi|x|^{\mu+1}} e^{|x|/2} \int\limits_{-\infty}^{\infty} \frac{|t|^{\mu}\cos t}{1+4\frac{t^2}{x^2}}\,\mathrm{d}t\,. \tag{24}$$

At $x \to \infty$, the main term of integral (24) reads

$$\begin{aligned} \mathcal{V}_{\mu\mathrm{E}}(x\to\infty) \;&\approx\; -\frac{2\lambda}{\pi|x|^{\mu+1}} e^{|x|/2} \int\limits_{-\infty}^{\infty} |t|^{\mu}\cos t\mathrm{d}t \\ &=\; \frac{4\mu\lambda}{\pi}\frac{e^{|x|/2}}{|x|^{\mu+1}}\Gamma(\mu)\sin\frac{\pi\mu}{2}\,. \end{aligned} \tag{25}$$

The integral $\int_{-\infty}^{\infty} |t|^{\mu}\cos t\,\mathrm{d}t$ exists because of presence of trigonometric function in it. It is calculated by infinitesimal shift of the variable t to the complex axis $t \to t + i\delta$ with subsequent limit $\delta \to 0$. Similar to the case of Gaussian pdf, here $e^{|x|/2} = 1/\sqrt{2\rho^*}$, which gives

$$(\rho^*)_{\mathrm{E}}^{1/2}(x\to\infty) \approx \frac{2\sqrt{2}\mu\lambda}{\pi}\frac{\Gamma(\mu)\sin\frac{\pi\mu}{2}}{|x|^{1+\mu}\mathcal{V}_{\mu\mathrm{E}}(x)}\,. \tag{26}$$

Expression (26) represents the desired asymptotics (along with the coefficient before the leading term) for exponential target. Our analysis shows that the asymptotic relations (23) and (26) are valid at approximately $|x| > 10$ for all $0 < \mu < 2$. Moreover, the above asymptotic expressions are not valid exactly at the points $\mu = 0$ and 2 in accord with the definition of fractional Laplacian (7).

4. Numerical simulations of semigroup dynamics in the derived potentials

In this section, we are going to solve numerically the equation for the so-called fractional diffusion (or topological diffusion as it used, in particular, to describe the topology of polymer chains, see, *e.g.* Refs. [29–32])

$$\partial_t\theta_* = -\lambda|\Delta|^{\mu/2}\theta_* - \mathcal{V}(x)\theta_* \tag{27}$$

with the potential functions $\mathcal{V}(x)$ in forms of (15) and (18) respectively. Here, $\theta_* \equiv \theta_*(x,t)$ is a conjugated "wave function", *cf.* Eq. (1). It is related

to transient pdf $\rho(x,t)$ as $\theta_*(x,t)\theta(x,t) = \rho(x,t)$, see below. We will call the dynamics with potential (15) (generated by Gaussian function) as *Gaussian dynamics*, while that with potential (18) (generated by exponential function) as *exponential dynamics*. Note that similar to Refs. [12] and [20], here we deal with discontinuous, jump-type processes. We recollect that the function $\mathbb{M}_\nu(x)$ is here strongly engaged as both above terminal pdfs (and hence semigroup potentials, determining the dynamic behavior) are expressed through it. Below, we consider the numerical solution of equation (27) (recasted to the equation for pdf $\rho(x,t)$) with initial density, which is also related to $\mathbb{M}_\nu(x)$, namely two-peaked δ-like function $\mathbb{M}_{\nu\to 1}(x)$.

Note also that, to the best of our knowledge, the present consideration is the first one to study the implications of $\mathbb{M}$-Wright function in the realistic physical problems with potentials, confining corresponding Lévy flights. This is because usually (see above) this function is related to the solution of the free diffusion problem with fractional time derivative. Below, we will point to the real physical problems, where our numerical solutions will be useful.

As the potential $\mathcal{V}(x)$ depends unambiguously on the terminal pdf $\rho_*(x)$, we reduce equation (27) to the form independent of $\mathcal{V}$. This permits to avoid the direct numerical representation of the hypergeometric functions (which is quite involved), substituting it by numerical calculation of corresponding fractional derivatives. Following [12], we define the potential $\Phi(x)$

$$\Phi(x) = \ln \rho_*^{1/2}(x)\,. \tag{28}$$

This substitution generates the effective Gibbs–Boltzmann form of the fractional diffusion equation (27), see Ref. [12] for details. In this case,

$$\theta^*(x,t) = \rho(x,t)\exp(-\Phi(x)) \equiv \frac{\rho(x,t)}{\rho_*^{1/2}(x)} \text{ and } \theta(x,t) = \rho_*^{1/2}(x) = \exp(\Phi(x))\,, \tag{29}$$

where now $\rho(x,t)$ is the desired transient pdf, for which we should solve the corresponding fractional equation. To obtain the form of this equation, we use the root of Refs. [12, 20] and substitute expression (29) for $\theta^*(x,t)$ into equation (27) to obtain

$$\partial_t \rho = -\lambda \exp(\Phi)|\Delta|^{\mu/2}\left[\rho\exp(-\Phi)\right] + \lambda\rho\exp(-\Phi)|\Delta|^{\mu/2}\exp(\Phi)\,. \tag{30}$$

Equation (30) is a desired equation for topological fractional diffusion, which does not contain the potential $\mathcal{V}(x)$. However, the substitution $\Phi(x) = -\kappa V(x)$ ($\kappa = (k_\mathrm{B}T)^{-1}$, k_B is Boltzmann constant, T is a temperature) recasts this equation to more customary (in polymer science) form [30–32].

We have

$$\frac{1}{\lambda}\partial_t\rho = -\exp\left(-\frac{\kappa V}{2}\right)|\Delta|^{\mu/2}\left[\rho\exp\left(\frac{\kappa V}{2}\right)\right] + \rho\exp\left(\frac{\kappa V}{2}\right)|\Delta|^{\mu/2}\left[\exp\left(\frac{-\kappa V}{2}\right)\right], \tag{31}$$

where explicitly

$$V(x) = -\frac{1}{\kappa}\ln\rho_*(x)\,. \tag{32}$$

Equation (31) (with respect to (32)) will be used in actual numerical calculations. Knowing the target function $\rho_*(x)$, we can effectively recover the potential in which fractional dynamics occur. In other words, knowing $\rho_*(x)$ and starting from any desired (taken, say, from physical grounds) initial function $\rho_0(x)$, we can trace the whole dynamical transition from $\rho_0(x)$ to $\rho_*(x)$ through intermediate steps $\rho(x,t)$.

As in numerical solution of Eq. (31), we use very small time steps, the simple Euler scheme for time derivatives is sufficient. Moreover, for fine spatial grid, it is sufficient to use trapezoid rule for evaluation of Cauchy principal value of integrals on each Euler time step for evaluation of fractional derivative $|\Delta|^{\mu/2}$.

We begin our numerical simulations with Gaussian dynamics. Equation (31) has been solved numerically for $\lambda = \kappa = 1$ and representative values of $\mu = 0.1$, 0.5, 1.0 and 1.5 for the initial function in the form of

$$\rho_0(x) = \frac{1}{2}\mathbb{M}_{0.96}(x)\,. \tag{33}$$

The dynamics is reported in Fig. 4. It is seen that for confining potential (15), the equilibrium is achieved quite quickly — already at $t = 0.8$ (for the slowest case of $\mu = 0.1$), the pdf arrives at terminal one and then stays constant in time. At the increase of Lévy index μ, the relaxation becomes faster. While at $\mu = 0.1$, the function $\rho(x, t = 0.01)$ is nearly the initial one, at $\mu = 1.5$, this function is almost at final stage of time evolution as equilibrium is achieved at $t = 0.1$ (it is seen that $\rho(x, t = 0.05)$ is already very close to $\rho_*(x)$). In other words, the increase of the parameter μ leads to effective equilibration of the probability distributions. To show that, we plot additional curves $\rho(x, t = 0.05)$ at $\mu = 1$ and 1.5 and $\rho(x, t = 0.005)$ at $\mu = 1.5$.

Although potential (18) for exponential dynamics has much more complex numerical realization than that for Gaussian one, the algorithm, based on equation (31), permits to calculate the time evolution quite easily. Once more, we start with $\rho_0(x)$ in the form of (33) and represent the results of

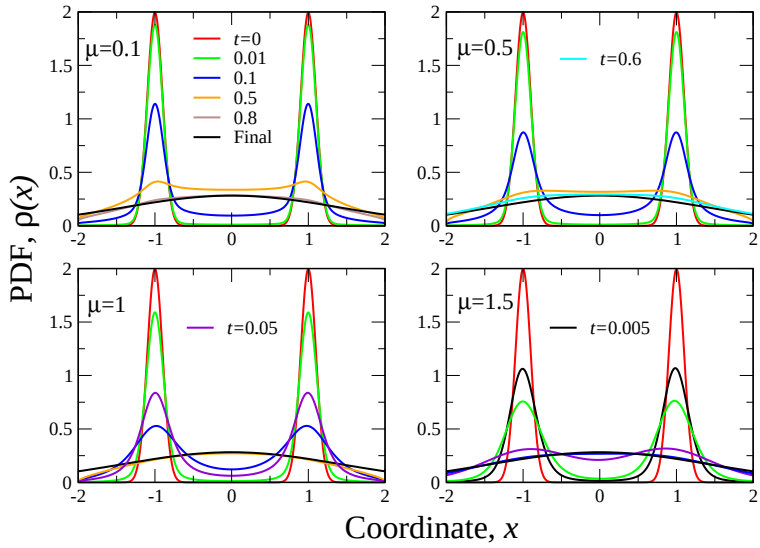

Fig. 4. (Colour on-line) The time evolution of pdfs $\rho(x,t)$ for Gaussian dynamics at different time instants t (coded by colors or by shadows of grey, see legends) and Lévy indices μ, shown in the panels. Both initial (red or light grey two-peaked curves, $t=0$) and final (target; black color) pdfs are also shown.

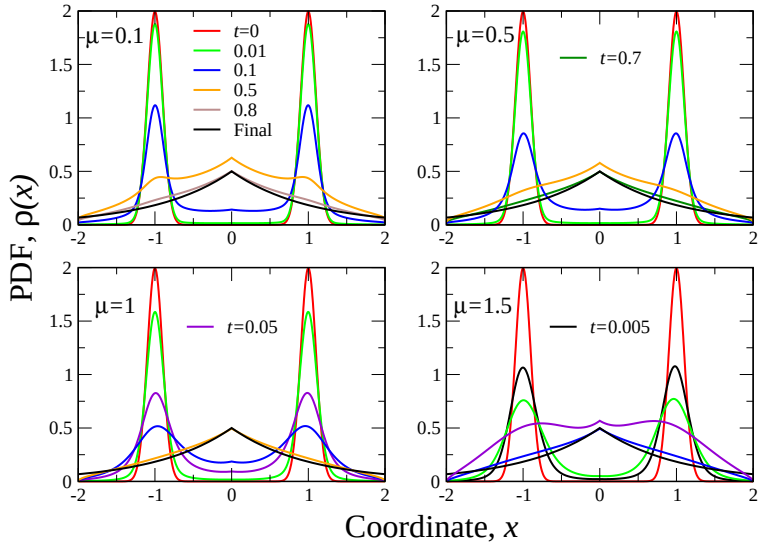

Fig. 5. (Colour on-line) The time evolution of pdfs $\rho(x,t)$ for exponential dynamics at different time instants t (coded by colors or by shadows of grey, see legends) and Lévy indices μ, shown in the panels. Both initial (red or light grey two-peaked curves, $t=0$) and final (terminal or equilibrium; black color) pdfs are also shown.

the numerical simulations in Fig. 5. The main features of that dynamics are similar to the Gaussian case. The only difference is that the target pdf has (as it should be) the cusp at $x = 0$. This implies that transient pdfs for large time instants (*i.e.* when pdf is close to final one) have also cusps at $x = 0$. Our analysis shows that these cusps are also responsible for potential (18) peculiarities (deep narrow wells) near $x = 0$, see Fig. 3.

Note that there is no problem to calculate numerically the dynamics of pdf for any other (then (33)) initial one. Moreover, any kind of target pdf (for example, $\mathbb{M}$-Wright function for arbitrary index ν) can be considered within the above algorithm. This is because there is no need now to have the analytical expression for the potential $\mathcal{V}(x)$, while the function $\mathbb{M}_\nu(x)$ can be effectively represented by power series for virtually any (at least at $\nu < 0.96$) index ν, see Fig. 1.

5. Summary

One of the reasons we choose the initial pdf in the form of (33) is that it might be used for the description of complicated magnetic resonance lineshapes, see, for instance, Fig. 10 of Ref. [22]. Actually, many more realistic processes (ranging from solid state physics, polymer chemistry and econophysics to marine biology and even contaminants spreading [33]) can be described by nonlocal fractional dynamics. We emphasize here, that in spite of that one of our considered pdfs is Gaussian, the presented formalism is suitable at its best to describe the jump-type non-Gaussian stochastic processes. Of course, the Gaussian one is also a particular case (for instance, through $\mathbb{M}$-Write function [14, 15]) of above class.

Let us finally say more about realistic physical regimes, where the above formalism can be applied. Standard examples here are the dynamical responce of amorphous materials such as conventional glasses (see, *e.g.*, Ref. [34]), the long-time relaxation in spin [34, 35], so-called orientational glasses [36] and especially crossover between glassy (non-Gaussian and possibly bimodal, two-peaked pdfs) and ordered (*e.g.* ferromagnetism in spin systems with Gaussian pdf) states. It had also been shown (see Refs. [37, 38]) that random electric fields, acting between dipole impurities in different kinds of disordered dielectrics, generate long-time nonexponential relaxation in them. Here, also the crossover from Gaussian to non-Gaussian relaxation patterns occurs.

This relaxation is a source of many experimentally observed anomalies. One more important application is the theory of inhomogeneously broadened resonant lines [39]. Such broadening occurs in condensed matter and/or biological species, in a number of spectroscopic manifestations such as the electron paramagnetic resonance, nuclear magnetic resonance, optical and

neutron scattering measurements, see, *e.g.* [39]. The broadening appears due to random electric and magnetic fields, strains and other perturbations from defects in a substance containing the centers whose resonant transitions between energy levels are studied. The usual technique of calculation of shapes of such resonant lines is the so-called statistical method [39, 40]. This method determines the line shape as an averaged (over spatial and thermal fluctuations) delta-function, stemming from the resonance contribution of each single center. The outcomes depend strongly on the spatial positions of the centers, their concentration, and interactions between them [40]. In this case, Gaussian pdf realizes for high centers concentration and strong short-range interaction between them. The opposite limiting case refers to small center concentrations and long-range (like dipole–dipole or higher multipole) interactions. It generates the long-tailed, non-Gaussian pdfs and Lorentz (Cauchy) distribution in particular. The intermediate regimes yield various non-Gaussian pdfs, with the Holtzmark function among them [40, 41]. Note that the application of the above formalism to the models of galaxy formation [42, 43] permits to answer a question about the possible ordering of angular momenta of smaller galaxies prior to their merging in larger objects [43]. The application of the considered dynamic formalism to the primordial time evolution of galaxies and their clusters may also permit to answer many yet unsolved questions. We shall discuss this important problem in the future publications.

Long-time experimental research on resonant techniques confirms the efficiency of statistical method in determination of the resonant line shapes, which generally are by no means Gaussian. The presented consideration shows that many physical systems are characterized intrinsically by transitions between Gaussian and non-Gaussian pdfs. In many cases, they can be obtained (through transient pdfs like the above obtained numerical results) from Gaussian pdf by varying the system parameters, like defects concentration, their type as well as external stimuli, such as temperature, pressure, electric or magnetic field *etc.* Note that, as our present analysis shows, the system can well finish with the Gaussian distribution. Namely, under suitable confining conditions, generated by the potential (depending on target pdf, see above), stemming, in its turn, from the unavoidable defects and impurities or external pressure in a sample, the initial non-Gaussian pdf (corresponding in our case to quite complicated bimodal pdf (33)) can relax to Gaussian.

REFERENCES

[1] D. Applebaum, *Lévy Processes and Stochastic Calculus*, Cambridge University Press, 2004.

[2] A. Lasota, M.C. Mackey, *Fractals and Noise: Stochastic Aspects of Dynamics*, Springer-Verlag, Berlin 1995.

[3] Z. Schuss, *Theory and Applications of Stochastic Processes: An Analytical Approach*, Springer, New York 2009.

[4] N.G. Van Kampen, *Stochastic Processes in Physics and Chemistry*, 3rd edition, North-Holland, Amsterdam 2007.

[5] R.N. Mantegna, H.E. Stanley, *Introduction to Econophysics: Correlations and Complexity in Finance*, Cambridge University Press, Cambridge 2007.

[6] S. Rachev, Y. Kim, M. Bianchi, F. Fabozzi, *Financial Models with Levy Processes and Volatility Clustering* Wiley, New York 2011.

[7] J.W. Kirchner, X. Feng, C. Neal, *Nature* **403**, 524 (2000).

[8] H. Scher *et al.*, *Geophys. Res. Lett.* **29**, 1061 (2002).

[9] O. Benichou, C. Loverdo, M. Moreau, R. Voituriez, *Rev. Mod. Phys.* **83**, 81 (2011).

[10] I.I. Eliazar, M.F. Shlesinger, *Phys. Rep.* **527**, 101 (2013).

[11] W.H. Lee, K.I. Hopcraft, E. Jakeman, *Phys. Rev. E* **77**, 011109 (2008).

[12] P. Garbaczewski, V. Stephanovich, *Phys. Rev. E* **80**, 031113 (2009).

[13] P. Garbaczewski, V. Stephanovich, *Physica A* **389**, 4419 (2010).

[14] R. Gorenflo, Yu. Luchko, F. Mainardi, *Fract. Calc. Appl. Anal.* **2**, 383 (1999) [arXiv:math-ph/0701069].

[15] F. Mainardi, A. Mura, G. Pagnini, *Int. J. Differential Equations* **2010**, 104505 (2010).

[16] E.M. Wright, *J. London Math. Soc.* **8**, 71 (1933).

[17] E.M. Wright, *Proc. London Math. Soc.* **38**, 257 (1935).

[18] E.M. Wright, *J. London Math. Soc.* **10**, 286 (1935).

[19] M. Abramowitz, I. Stegun (Eds.), *Handbook of Mathematical Functions*, Dover, New York 1972.

[20] P. Garbaczewski, V. Stephanovich, *Phys. Rev. E* **84**, 011142 (2011).

[21] H.J. Haubold, A.M. Mathai, R.K. Saxena, arXiv:0909.0230 [math.ca].

[22] Yu.O. Zagorodnii *et al.*, *Phys. Rev. Mater.* **2**, 014401 (2018).

[23] S.G. Samko, A.A. Kilbas, O.I. Maritchev, *Fractional Integrals and Derivatives*, Gordon and Breach, New York 2003.

[24] P. Garbaczewski, R. Olkiewicz, *J. Math. Phys.* **40**, 1057 (1999).

[25] I. Eliazar, J. Klafter, *J. Stat. Phys.* **111**, 739 (2003).

[26] P. Garbaczewski, V.A. Stephanovich, *Acta Phys. Pol. B* **43**, 977 (2012).

[27] K. Kaleta, J. Lorinczi, *Phys. Rev. E* **93**, 022135 (2016).

[28] K. Kaleta, T. Kulczycki, *Potential Analysis* **33**, 313 (2010).
[29] D. Brockmann, I. Sokolov, *Chem. Phys.* **284**, 409 (2002).
[30] D. Brockmann, T. Geisel, *Phys. Rev. Lett.* **90**, 170601 (2003).
[31] D. Brockmann, T. Geisel, *Phys. Rev. Lett.* **91**, 048303 (2003).
[32] V.V. Belik, D. Brockmann, *New J. Phys.* **9**, 54 (2007).
[33] J.W. Kirchner, X. Feng, C. Neal, *Nature* **403**, 524 (2000).
[34] G. Parisi, *Field Theory, Disorder and Simulations*, World Sci., Singapore 1992.
[35] K. Binder, A.P. Young, *Rev. Mod. Phys.* **58**, 801 (1986).
[36] U.T. Höchli, K. Knorr, A. Loidl, *Adv. Phys.* **39**, 405 (1990).
[37] V.A. Stephanovich, *Ferroelectrics* **192**, 29 (1997).
[38] E.V. Kirichenko, V.A. Stephanovich, *Acta Phys. Pol. B* **43**, 1027 (2012).
[39] A. Abragam, *Principles of Nuclear Magnetism*, Oxford University Press, 2002.
[40] A.M. Stoneham, *Rev. Mod. Phys.* **41**, 82 (1969).
[41] S. Chandrasekhar, *Rev. Mod. Phys.* **15**, 1 (1943).
[42] M.S. Longair *Galaxy Formation*, Springer, Berlin 2008.
[43] V.A. Stephanovich, W. Godłowski, *Astrophys. J.* **810**, 167 (2015).